Inhomogeneous spatial distribution of non radiative recombination centers in GaN/InGaN nanowire heterostructures studied by cathodoluminescence

Alexandre Concordel, Névine Rochat, Anh My Nhat Quach, Jean-Luc Rouvière, Gwénolé Jacopin, Jérôme Napierala, Bruno Daudin

Inhomogeneous spatial distribution of non radiative recombination centers in GaN/InGaN nanowire heterostructures studied by cathodoluminescence

Abstract

In order to elucidate the mechanisms responsible for cathodoluminescence intensity variations at the scale of single InGaN/GaN nanowire heterostructures, a methodology is proposed based on a statistical analysis on ensembles of several hundreds of nanowires exhibiting a diameter of 180, 240 and 280 nm. For 180 nm diameter, we find that intensitiy variations are consistent with incorporation of point defects obeying Poisson's statistics. For wider diameters, intensity variations at the scale of single NWs are observed and assigned to local growth conditions fluctuations. Finally, for the less luminescent nanowires, a departure from Poisson's statistics is observed suggesting the possible clustering of non independent point defects.

InGaN/GaN layered heterostructures have now become a mature solution for solid state lightning. As a matter of fact, the external quantum efficiency (EQE) of devices may be as high as 90% in the blue range[1]. However, this efficiency is continuously decreasing for increasing wavelength emission putting in evidence that room still remains for improvement. The increasing dislocation density and internal electric field are among the reasons usually invoked to account for the decreasing EQE related to the increasing InN molar fraction of InGaN quantum wells (QWs) when targeting at long wavelength emission. In addition, the formation of both intrinsic and extrinsic point defects was identified as another source of non-radiative recombination centres (NRCs) affecting EQE[2]. The formation of complexes associating intrinsic and native point defects as well as extrinsic point defects and dislocations was also pointed out both theoretically and experimentally[2,3].

With the purpose of limiting defect formation on the surface of GaN layers grown by molecular beam epitaxy (MBE), the surfactant effect of In was found to improve both surface morphology and structural quality of GaN layers, which was assigned to modifications of surface kinetics[4]. The improvement of optical properties of GaN layers doped with In was later attributed to the suppression of NRCs associated with these In-induced kinetics modifications[5] .

More recently, the deposition of InGaN layers below the active InGaN/GaN QWs active region was found to drastically improve radiative recombination[6]. This effect was assigned to the trapping of NRCs generated at interfaces during growth interruptions. More generally, the experimental evidence of the presence of point defects in InGaN/GaN heterostructures has motivated the development of a strategy to prevent their detrimental effect on radiative efficiency. The trapping of point defects by an InGaN underlayer (UL) was proposed to account for the decrease of the Shockley-Read-Hall (SRH) non radiative recombination coefficient and the concomitant increase of radiative recombination efficiency of InGaN/GaN QWs heterostructures grown by metalorganic vapour phase epitaxy (MOVPE)[7–11].

In this context, the current interest in InGaN/GaN nanowire (NW) heterostructures is partly motivated by the expected elimination of the non-radiative recombination channel associated with extended defects as well as by the decrease of quantum confined Stark effect (QCSE) resulting from the eased strain relaxation and decrease of internal electric field[12]. As concerns the issue of point defects, the concept of UL was recently applied to InGaN/GaN NW heterostructures grown by MBE. It led to a significant improvement of luminescence efficiency, which was ascribed to the trapping of point defects generated in the GaN pillar template grown by MOVPE[13]. Nevertheless, the occurrence of an additional non-radiative mechanism associated with the MBE step itself was put in evidence and tentatively assigned to the incorporation of intrinsic and/or extrinsic point defects during the growth of the

InGaN/GaN NWs heterostructures. In particular, the experimental evidence of a more luminescent shell surrounding a less luminescent core was consistent with local fluctuations of metal adatom density on the growth front[13], in accordance with theoretical predictions emphasizing the importance of growth conditions on extrinsic impurities incorporation and/or intrinsic defect formation[14].

The goal of the present study was to shed light on the incorporation mechanism of such point defects by performing a statistical analysis of the cathodoluminescence (CL) intensity of collections of several hundreds of regularly ordered InGaN/GaN NW heterostructures, as a function of their diameter. Assuming that non radiative point defect random incorporation obeys Poisson statistics, it was possible to quantitatively estimate the number of defects incorporated in the active region, ranging from about one ten to a few tens per NW.

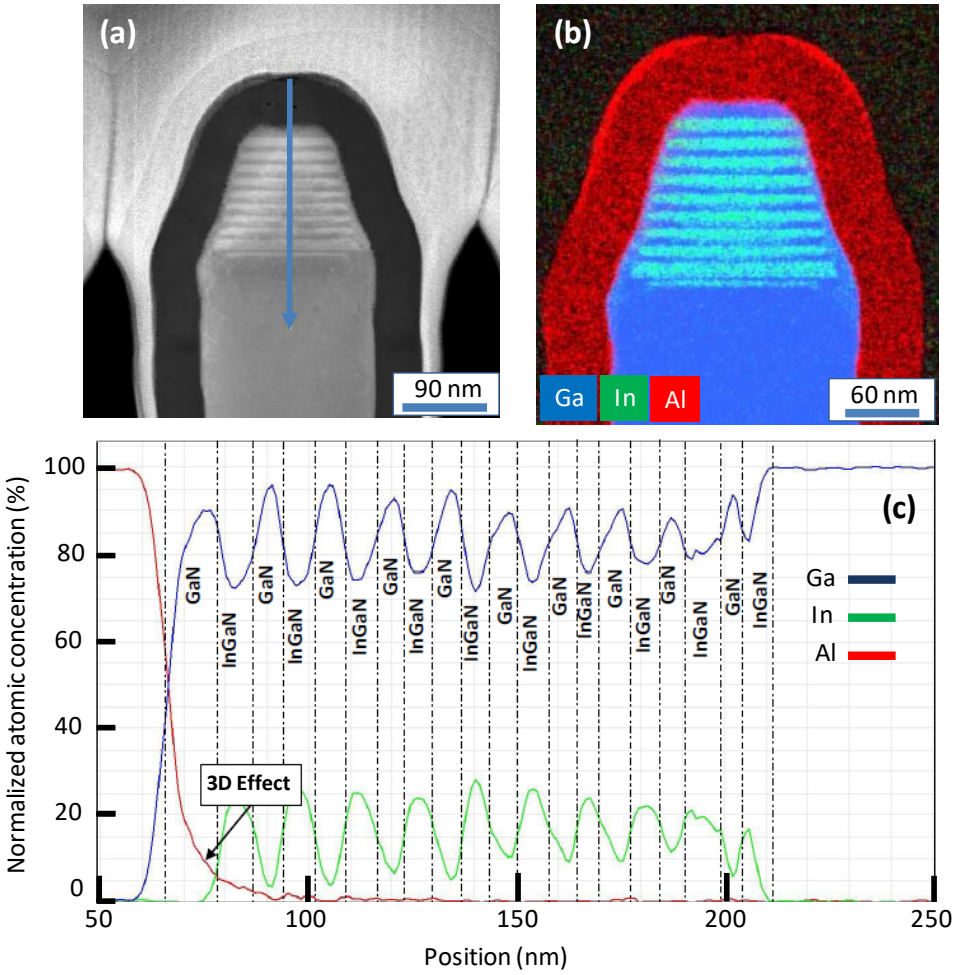

Figure 1: (a) FIB lamella of the InGaN/GaN nanowire heterostructure (diameter 180 nm). (b) EDX mapping of Ga, In and Al. Al corresponds to the AlO_x protective layer. (c) EDX profile along the arrow shown in (a). Note that the Al atomic concentration profile extension till 100 nm is an artefact assigned to the 3D character of the nanowire heterostructure.

The pseudo-templates used in this study consist of ordered arrays of MOCVD-grown GaN NWs elaborated by selective area growth (SAG) on a sapphire substrate covered by a 5 μm, Ga-polar n-doped GaN buffer layer. A 40 nm SiN mask was deposited by low pressure chemical vapor deposition, and next patterned by e-beam lithography, to realize homogeneous arrays of holes with different diameters for in-plane ordered growth of GaN NWs with diameters ranging from 135 nm to 280 nm. The NWs spacing was 400 nm. After introduction in the PA-MBE growth chamber, the pseudo-templates were out-gassed at 950°C during 45 min before further deposition of the MBE-grown section, which consisted of a 25-nm thick GaN layer, deposited on the pseudo-template, followed by the growth of a nominally 50 nm thick InGaN UL with an In content of about 3% and a 20-nm thick GaN spacer. The purpose of the UL was to trap point defects segregated at the surface of the MOCVD template, preventing their further incorporation in the MBE-grown section[13]. On top of the GaN spacer, multi-quantum wells (MQWs) were grown, consisting of an $In_xGa_{1-x}N$/GaN sequence repeated ten times. Three diameters were investigated in detail, namely 180, 240 and 280 nm. The emission wavelength of the MQWs was around 490 nm, independent of diameter. In the case of the 180 nm diameter NWs, the InN molar fraction was determined by energy dispersive X ray spectroscopy (see figure 1) and was around 20%. Also shown in figure 1, the In profile along the growth axis clearly reveals that the first (second) QW is thinner (thicker) than the average. We assign this feature to a strain-governed delay in In incorporation in the first QW, resulting in In accumulation on the surface and thickening of the second QW. This interpretation is supported by the evidence of increasing In content from first to fourth QW, followed by a steady state regime and a roughly constant In content. This is consistent with a strain pulling effect, i.e. a balance between strain and In content till elastic relaxation to an equilibrium value.

First,CL and time-correlated measurements were performed at room temperature in an FEI Inspect F50 SEM. The acceleration voltage has been set to 5 kV ensuring a penetration depth of 160 nm in GaN and 145 nm in InGaN with a 20% InN molar fraction (CASINO software simulation) to only probe the MBE QW regrown section.. A Horiba Jobin Yvon ihR550 spectrometer equipped with a photomultiplier tube detector centered at the active region spectral region was used for spectral analysis. Concerning the time correlation CL measurements, detailed information can be found in Ref [15].

Figure 2a shows a CL mapping of the sample in a region consisting of NWs exhibiting a diameter of 180 nm. It is observed that CL of each NW is spatially homogeneous, however, marked CL intensity variations are observed from NW to NW. In order to probe the recombination dynamics, time correlated–CL (TC-CL) experiments were performed on a series of individual NWs identified in figure 2a. The result is displayed in figure 2b, putting in evidence marked differences in effective lifetime value from NW to NW. Data in figure 2c obtained for a statistically significant number of NWs point towards a linear correlation between the effective lifetime value and the CL intensity. It was further found that the emission wavelength was constant as a function of CL intensity. This allows us to rule out wavelength variation as a factor influencing both the lifetime and intensity of CL (see discussions in

supplementary material). Thus, the observed wire-to-wire lifetime variation is directly related to the variation in the density of the NR centre.

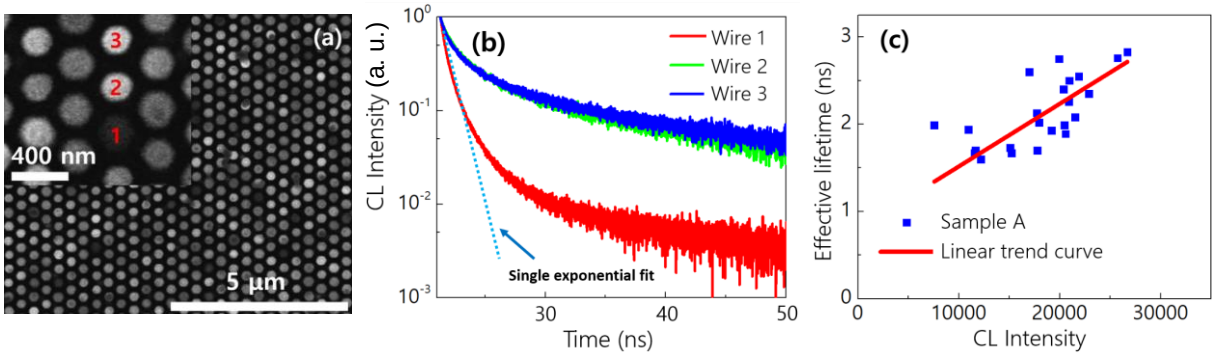

Figure 2: (a) CL mapping of 180 nm diameter NWs at the active region wavelength range. Inset: zoomed image. (b) CL evolution as a function of time for the three NWs shown in inset in (a). (c) CL lifetime as a function of CL intensity, assessing their linear relationship.

The statistical analysis of CL intensity on an ensemble of about 500 NWs of 180 nm is shown in figure 3. For each NW in figure 2a, a circle was defined and the intensity was summed over all pixels enclosed in it, leading to one histogram shown in figure 3a, which represents the CL intensity distribution of such NWs (more details in Fig. S2 in supplementary material). Next, as shown in figure 3b, the x axis was chosen for convenience so that it expends from maximal CL intensity value to the minimal one. In this representation, based on the previous established correlation between CL intensity and R/NR recombination ratio, and knowing that the CL intensities measured are not absolute values, the highest CL intensity level corresponds to NWs of the population under scrutiny containing the lowest number of NR defects. Conversely, the lowest CL intensity level corresponds to NWs containing the highest number of NR defects. It is then possible to plot a cumulative distribution function of the number of NWs as a function of the normalized number of NRCs, which is shown in figure 3b. For example, it is seen that 75% of the NWs contain half or less of the maximal number of defects.

The possible NRCs responsible for the observed CL intensity variation include extended defects such as dislocations and intrinsic or extrinsic point defects. However, if present, misfit dislocations resulting from InGaN/GaN lattice mismatch should affect each NW in the same way, making doubtful their role on the widely dispersed CL intensity fluctuations. By contrast, point defects such as chemical impurities or N/metal vacancies could be candidates responsible for the random intensity fluctuations observed at large scale. In particular, chemical impurities limiting base vacuum in MBE, such as O, C, H and others can be viewed as an equivalent atomic flux impinging on the growing surface. Then the incorporation of such extrinsic chemical impurities is expected to obey Poisson statistics, accounting for the discrete occurrence of independent incorporation events at constant mean rate. The probability law of a random variable X following a Poisson law of parameter λ is given by (1):

$$P(X = k) = \frac{\lambda^k}{k!} e^{-\lambda} \qquad (1),$$

with k being one occurrence, corresponding here to a defect incorporated in the active region during the growth, λ the Poisson law parameter, which corresponds to the average number of defects incorporated in the heterostructure, and P(X = k) the probability that k defects have been incorporated in the active region.

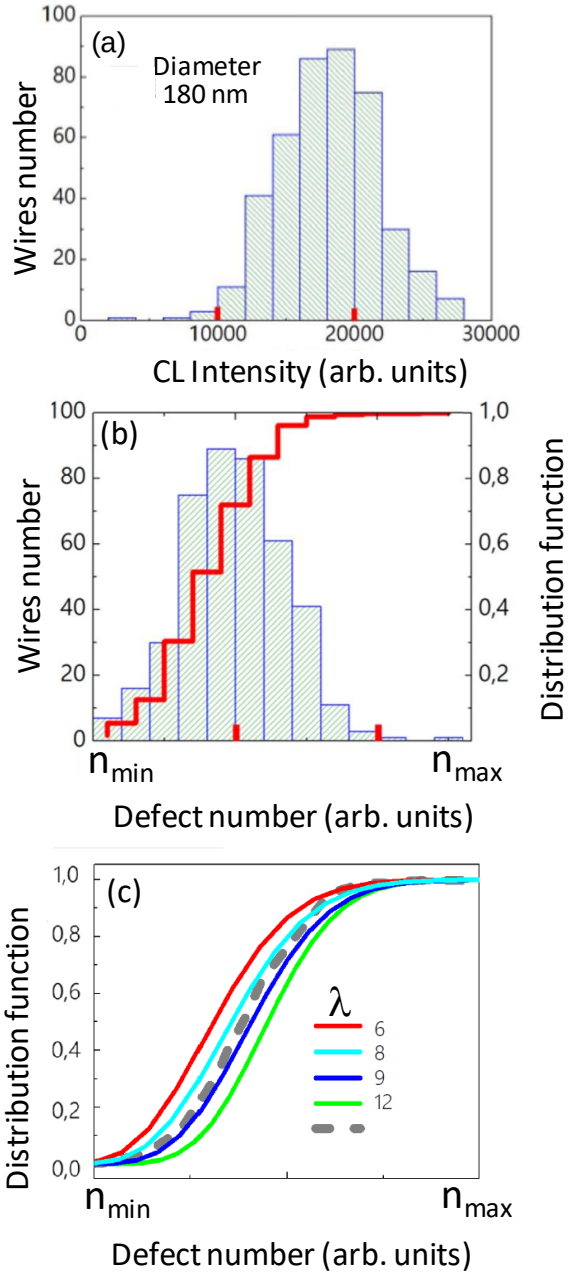

Figure 3: a) Intensity distribution histogram of 180 nm NWs shown in figure 1a. (b) Inverted histogram. n_{min} corresponds to most luminescent NWs, n_{max} to less luminescent ones. Red: distribution

function (c) distribution functions for different λ parameters values. Grey dashed line: experimental distribution function extracted from (b).

Several distribution functions of the Poisson law are plotted in figure 3c, for different λ values (solid lines), along with the integrated distribution function experimentally obtained from the 180-nm diameter NWs CL mapping. As experimental CL maps were performed on about 500 NWs, n_{min} and n_{max} were defined by considering the lowest luminescence intensity probability value experimentally significant. This value refers to one single NW from the collection under scrutiny, i.e. $1/500 = 2.10^{-3}$ for n_{min} and $(1- 1/500) = (1- 2.10^{-3})$ for n_{max}. The satisfactory agreement between the distribution function variations and the theoretical modelling supports the hypothesis that the incorporation of non radiative defects during growth mostly obeys Poisson statistics for 180 nm NWs.

The same method was performed on an ensemble of about 500 NWs exhibiting a diameter D of 240 and 280 nm. For these larger diameters, it is visible in figure 4a that the periphery of single NWs is more luminescent than the core. This feature was investigated in a previous study and assigned to metal adatom coverage variations on top of growing NWs[13]. More precisely, the metal flux impinging on the side walls and diffusing towards top tends to accumulate at the NW top periphery[16]. In consequence it is speculated that metal coverage indeed drastically affects the point defect incorporation/formation mechanism. Interestingly, the distribution function of the periphery part of the NWs with 240 and 280 nm diameters varies similarly to the distribution function of NWs exhibiting a 180 nm NWs, suggesting a similar point defect density in both cases. By contrast, in the central part, the distribution function is shifted to the right, indicative of a larger density of point defects. Furthermore, for large diameters, a significant departure from theoretical curves is observed in the range of high defect number / lowest CL intensity, associated with the darker NWs in figure 4a. This is possibly due to the fact that defects, if numerous enough, cannot be viewed as independent NRCs. Alternately it may suggest that another source of NRCs not obeying Poisson's statistics such as dislocations could account for the weak CL emission of the less luminescent NWs.

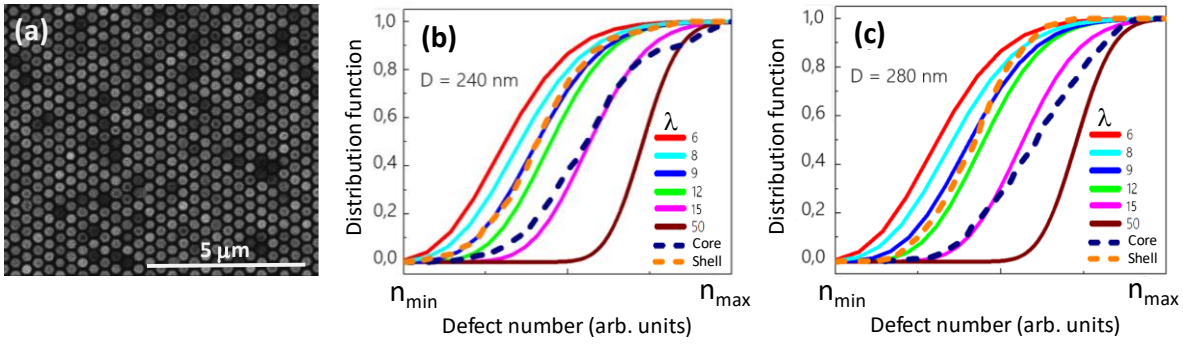

Figure 4: (a) CL intensity mapping of the 240 nm diameter NWs integrated in the 480-500 nm spectral range. (b) Full lines: theoretical distribution function for various λ parameter values ranging

from 6 to 50. Dashed lines: statistical analysis of core (dark blue) and shell (orange) CL intensity) for D= 240 nm NWs. (c) The same for D= 280 nm NWs.

With the purpose of clarifying this issue, cross section low temperature CL hyperspectral mapping was performed on one NW in a lamella extracted from the 180 nm NW sample, which was prepared by focused ion beam (FIB). For these experiments, an Attolight Allalin system with a fully integrated -in axis-achromatic-high numerical aperture- optical collection was used. Figure 5a shows the secondary electron image of the NW obtained simultaneously to CL spectra, which were acquired using 10kV acceleration voltage, 10nA beam current and 200 ms integration time for each pixel. These excitation conditions and the reduced thickness of the specimen ensure a CL spatial resolution of about 20 nm. CCD detection allows acquisition of CL hyperspectral maps in the whole range of interest. Figures 5b, 5c and 5d show maps recorded at 367nm, 436nm and 487nm that correspond to GaN, underlayer, quantum well emission energy, respectively. Interestingly, the extension of the 436 nm UL-related signal is larger than the nominal UL thickness, which is assigned to carrier diffusion from GaN region towards the lower gap InGaN UL where they recombine. No core–shell CL intensity structure is detected on QW signal, consistent with results in figure 2 and the absence of such core-shell feature for 180 nm NWs. However, the core-shell CL intensity structure is visible for the UL and the GaN spacer area, while it is not detected in both MOCVD and MBE GaN section at the bottom of the NW. This suggests a common phenomenology between the CL intensity variations in InGaN QWs and those observed in figure 5, characteristic of the MBE-grown sections in the heterostructure. As the InN molar fraction in the UL lies in the 5-7 percent range, the formation of misfit dislocations in the GaN spacer is not expected for NWs with a 180 nm diameter[12]. Then the observation of a core-shell intensity distribution in the GaN section further supports the hypothesis of a relation to point defects rather than to extended structural defects. The same holds for the UL which is not expected to be plastically relaxed for the same reasons as for GaN section.

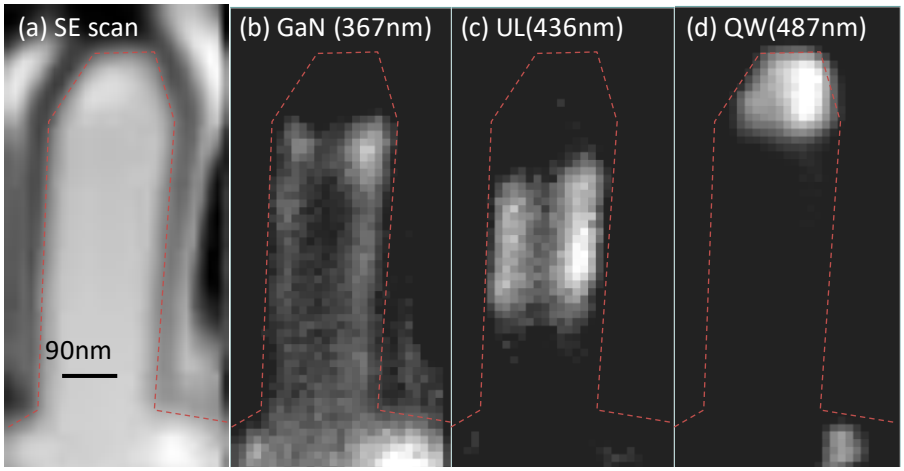

Figure 5: (a) secondary electron (SE) image of one NW extracted from the 180 nm NW sample investigated by CL. (b) CL mapping at 367 nm, corresponding to GaN near band edge. Note a core-shell CL intensity inhomogeneity in the GaN spacer area, which is absent in the bottom GaN section. (c) CL mapping at 436 nm, corresponding to the underlayer. (d)) CL mapping at 487 nm, corresponding to the InGaN/GaN QW section.

From the fit between data and theoretical curves in figure 3, the total concentration of defects normalized for each diameter, to the total volume of InGaN QWs in the heterostructureswas calculated and is shown in table 1. In the case of samples exhibiting a shell the defect concentration was independently calculated for both shell and core, normalized to the respective volume of each region. Accordingly, a defect concentration in shells of about $5.10^{15}/cm^3$ is found, while in the core, when present, it is about 15-20 times higher. Such point defect concentration values are consistent with the values reported by Weatherley et al[17]. Although their chemical nature is not clear at this stage, the dependence of the point defect density on local growth conditions, namely metal accumulation in the NW periphery which was discussed above, points towards the possible role of Ga vacancies (V_{Ga}). Actually, as discussed by Dreyer et al[18], the formation of complexes associating V_{Ga} with O and/or H is expected to be eased in InGaN, correlatively with a drastic increase of the Shockley-Read-Hall non radiative recombination coefficient. The defect density considered by these authors, namely $10^{16}/cm^3$, favourably compares with the estimates extracted from the present work, as a further clue that extrinsic point defects and/or intrinsic-extrinsic point defects complexes are likely responsible for the observed CL intensity fluctuations. However, it is worth stressing that the defect density in cores extracted from data in figure 4 is likely overestimated, as inferred from the departure from Poisson's statistics for poorly luminescent NWs. Also visible in figure 4, departure from Poisson's statistics is more marked for NWs with a 280 nm diameter than for those with a 240 nm diameter, as a clue that non-poissonian defects are indeed more numerous in NW heterostructures exhibiting a large diameter. This feature, supported by results in figure 5, further suggests that extended point defects such as partial dislocations associated with stacking faults[19], expected to be more favourably formed in large diameter NWs, might be partly responsible for the departure from Poisson statistics.

NW diameter (nm)	Defect conc. (shell)	Defect conc. (core)	Core/shell ratio
180	$5.9 \pm 1.1\ 10^{15}/cm^3$		-
240	$5.0 \pm 0.7\ 10^{15}/cm^3$	$1 \pm 0.7\ 10^{17}/cm^3$	20
280	$3.7 \pm 0.7\ 10^{15}/cm^3$	$5.6 \pm 1.9\ 10^{16}/cm^3$	15

Table 1: point defect density extracted from data in figures 3c, 4b and 4c

In conclusion, based on a linear correlation between CL intensity and luminescence decay time, a methodology was proposed to quantitatively investigate the nature of NRCs in InGaN/GaN NW heterostructures. In particular it was established that the CL variations from NW to NW in InGaN/GaN NW heterostructures emitting around 490 nm can be mostly assigned to the incorporation during growth of point defects obeying Poisson's statistics. Although the nature of these point defects is still unclear, chemical impurities incorporated during growth are likely candidates along with extrinsic defects such as metal or nitrogen vacancies, possibly forming complexes with chemical impurities. For NWs exhibiting a diameter larger than 180 nm, the observation of a less luminescent core and a more luminescent shell was tentatively assigned to inhomogeneous metal accumulation on the top, suggesting that a special care should be paid to growth conditions engineering for optimization of luminescence efficiency.

Acknowledgments:

References

[1] S. Marcinkevičius, R. Yapparov, Y.C. Chow, C. Lynsky, S. Nakamura, S.P. DenBaars, and J.S. Speck, Appl. Phys. Lett. **119**, 071102 (2021).
[2] J.L. Lyons, D. Wickramaratne, and C.G. Van de Walle, J. Appl. Phys. **129**, 111101 (2021).
[3] M. Meneghini, M. la Grassa, S. Vaccari, B. Galler, R. Zeisel, P. Drechsel, B. Hahn, G. Meneghesso, and E. Zanoni, Appl. Phys. Lett. **104**, 113505 (2014).
[4] F. Widmann, B. Daudin, G. Feuillet, N. Pelekanos, and J.L. Rouvière, Appl. Phys. Lett. **73**, 2642 (1998).
[5] H. Kumano, K. Hoshi, S. Tanaka, I. Suemune, X.-Q. Shen, P. Riblet, P. Ramvall, and Y. Aoyagi, Appl. Phys. Lett. **75**, 2879 (1999).
[6] T. Akasaka, H. Gotoh, T. Saito, and T. Makimoto, Appl. Phys. Lett. **85**, 3089 (2004).
[7] A.M. Armstrong, B.N. Bryant, M.H. Crawford, D.D. Koleske, S.R. Lee, and J.J. Wierer, J. Appl. Phys. **117**, 134501 (2015).
[8] C. Haller, J.-F. Carlin, G. Jacopin, D. Martin, R. Butté, and N. Grandjean, Appl. Phys. Lett. **111**, 262101 (2017).
[9] C. Haller, J.-F. Carlin, G. Jacopin, W. Liu, D. Martin, R. Butté, and N. Grandjean, Appl. Phys. Lett. **113**, 111106 (2018).
[10] A.Y. Polyakov, C. Haller, N.B. Smirnov, A.S. Shiko, I.V. Shchermerov, S.V. Chernykh, L.A. Alexnayan, P.B. Lagov, Yu.S. Pavlov, J.-F. Carlin, R. Butté, M. Mosca, N. Grandjean, and S.J. Pearton, J Appl Phys **126**, 125708 (2019).
[11] M. Buffolo, A. Caria, F. Piva, N. Roccato, C. Casu, C. De Santi, N. Trivellin, G. Meneghesso, E. Zanoni, and M. Meneghini, Phys. Status Solidi A **219**, 2100727 (2022).
[12] F. Glas, Phys. Rev. B **74**, 121302 (2006).
[13] A. Concordel, J. Bleuse, G. Jacopin, and B. Daudin, Nanotechnology **34**, 035703 (2023).
[14] C.G. Van de Walle and J. Neugebauer, J. Appl. Phys. **95**, 3851 (2004).
[15] S. Finot, C. Le Maoult, E. Gheeraert, D. Vaufrey, and G. Jacopin, ACS Photonics **9**, 173 (2022).
[16] M. Gruart, G. Jacopin, and B. Daudin, Nano Lett. **19**, 4250 (2019).
[17] T.F.K. Weatherley, W. Liu, V. Osokin, D.T.L. Alexander, R.A. Taylor, J.-F. Carlin, R. Butté, and N. Grandjean, Nano Lett. **21**, 5217 (2021).
[18] C.E. Dreyer, A. Alkauskas, J.L. Lyons, J.S. Speck, and C.G. Van de Walle, Appl. Phys. Lett. **108**, 141101 (2016).
[19] X. Zhang, B. Haas, J.-L. Rouvière, E. Robin, and B. Daudin, Nanotechnology **27**, 455603 (2016).